Journal of
Computational and Theoretical Nanoscience
Vol. 7, 1–7, 2010

Calculation of Fluctuations in Boundary Layers of Nanowire Field-Effect Biosensors

Clemens Heitzinger[1,*], Yang Liu[2], Norbert J. Mauser[1], Christian Ringhofer[3], and Robert W. Dutton[2]

[1] *Department of Mathematics and Wolfgang Pauli Institute, University of Vienna, Vienna, Austria*
[2] *Center for Integrated Systems, Stanford University, Palo Alto, California, USA*
[3] *Department of Mathematics, Arizona State University, Tempe, Arizona, USA*

Fluctuations in the biofunctionalized boundary layers of nanowire field-effect biosensors are investigated by using the stochastic linearized Poisson-Boltzmann equation. The noise and fluctuations considered here are due to the Brownian motion of the biomolecules in the boundary layer, i.e., the various orientations of the molecules with respect to the surface are associated with their probabilities. The probabilities of the orientations are calculated using their free energy. The fluctuations in the charge distribution give rise to fluctuations in the electrostatic potential and hence in the current through the semiconductor transducer of the sensor, both of which are calculated. A homogenization result for the variance and covariance of the electrostatic potential is presented. In the numerical simulations, a cross section of a silicon nanowire on a flat surface including electrode and back-gate contacts is considered. The biofunctionalized boundary layer contains single-stranded or double-stranded DNA oligomers, and varying values of the surface charge, of the oligomer length, and of the electrolyte ionic strength are investigated.

Keywords: Nanowire, Field-Effect Biosensor, Stochastic Poisson-Boltzmann Equation, Fluctuation, Noise, Multiscale Problem, Homogenization.

RESEARCH ARTICLE

1. INTRODUCTION

Affinity-based field-effect biosensors have been experimentally demonstrated recently.[1–3] The main advantage of this sensor type is label-free operation, whereas current technology works with fluorescent or radioactive labels. The basic idea of a field-effect sensor is that a semiconductor transducer is functionalized with receptor molecules and placed in an electrolyte. A schematic diagram is shown in Figure 1. When target molecules bind to the receptor molecules at the transducer surface, the partial charges of the target molecules change the charge concentration in the boundary layer and hence the electrostatic potential in the transducer. Therefore the conductance of the semiconductor transducer is changed as well and this change is measured as the read-out signal. These sensors are selective, since only matching target molecules can bind to the immobilized receptor molecules. The amount of conductance change yields quantitative information about the amount of target molecules at the sensor surface, and therefore these structures are sensitive as well. This sensor concept is also a very general one regarding the types of biomolecules that can be detected. For the detection of DNA, the surface is functionalized with single-stranded PNA (peptide nucleic acid) or DNA receptors. For the detection of other biomolecules, a suitable (monoclonal) antibodies are used, and various tumor markers have been detected in this way.[4]

Recently, we have presented PDE-based models and homogenized PDEs for the theoretic understanding of field-effect (bio-)sensors.[5–9] Still, questions about the physics of field-effect sensors remain open. Particularly, randomness and fluctuations are present in actual biosensors due to Brownian motion, i.e., the molecules change their orientation with respect to the sensor surface, and due to binding and unbinding of target molecules. Such inhomogeneity was previously shown to be critical in determining the input dynamic ranges of affinity-based biosensors using the Langmuir-Freundlich adsorption isotherm.[9] To model these fluctuations, it is therefore necessary to consider the ensemble of varying charge concentrations in the boundary layer and their associated probabilities.

This work is an extension of recent work.[10] Compared to the previous PDE-based models, we introduce a model based on a stochastic PDE for fluctuations or noise. The basic model equation is a stochastic elliptic PDE for the

*Author to whom correspondence should be addressed.

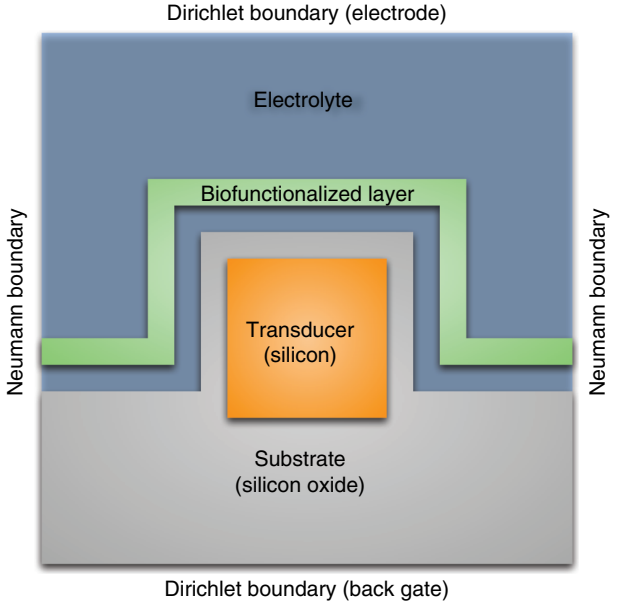

Fig. 1. Schematic diagram of the cross section of the nanowire field-effect biosensor considered here.

electrostatic potential in field-effect biosensors. The model can be applied to the electrostatics of similar structures and to other sources of noise in a straightforward manner. Here, our main goal is to investigate in numerical simulations how the stochastic charge concentrations in the boundary layer influence the current through the transducer.

The expectation of the electrostatic potential and its variance are calculated. Based on these, the expectation and variance of the current through a cross section of the transducer are obtained. The advantages of the stochastic-PDE model compared to Monte-Carlo simulations is the reduced computational effort. In a Monte-Carlo approach, many more solutions of the Poisson-Boltzmann equation would be required to just estimate the expectation and variance.

This work is organized as follows. In Section 2, the details of the model and its equations are described. In Section 3, results from the homogenization of the stochastic linearized Poisson-Boltzmann equation are presented and their significance for the variance is discussed. In Section 4, simulation results for a silicon-nanowire DNA sensor are presented. Finally, Section 5 concludes the paper.

2. THE MODEL EQUATIONS

2.1. The Stochastic Linearized Poisson-Boltzmann Equation

The basic model equation for the electrostatic potential $\phi(x,\omega)$ in the sensor considered here is the stochastic linearized Poisson-Boltzmann equation

$$-\nabla\cdot(A(x)\nabla\phi(x,\omega))+\gamma(x)\phi(x,\omega)=\rho(x,\omega) \qquad (1)$$

where ω is a random variable and $A(x)$ is the permittivity. The charge concentration on the right-hand side

$$\rho(x,\omega):=\rho_{\mathrm{f}}(x,\omega)+\alpha(x)$$

includes the fixed charge concentration $\rho_{\mathrm{f}}(x,\omega)$. The general form of the nonlinear Poisson-Boltzmann equation includes a Boltzmann distribution with Fermi level ϕ_{F} for the mobile charges in the electrolyte. The linearized equation is obtained by Taylor expansion around ϕ_0 from the nonlinear one. This linearization yields

$$\alpha(x):=2c(x)q\sinh\frac{q(\phi_{\mathrm{F}}-\phi_0)}{k_{\mathrm{B}}T}+\frac{2c(x)q^2\phi_0}{k_{\mathrm{B}}T}\times\cosh\frac{q(\phi_{\mathrm{F}}-\phi_0)}{k_{\mathrm{B}}T}$$

$$\gamma(x):=\frac{2c(x)q^2}{k_{\mathrm{B}}T}\cosh\frac{q(\phi_{\mathrm{F}}-\phi_0)}{k_{\mathrm{B}}T}$$

where $c(x)$ is the bulk concentration of the ions, q is the elementary charge, k_{B} is the Boltzmann constant, and T is the temperature.

The fluctuations or noise in the electrostatic potential due to the random variable ω are characterized by the expectation $E\phi$ and the variance $\sigma^2\phi$ of the potential. A PDE for the expectation $E\phi$ is found by the following argument. We define L to be the operator of the left-hand side of (1), i.e.,

$$L:=-\nabla\cdot(A(x)\nabla)+\gamma(x)$$

Since L and the expectation operator E commute at least formally, i.e.,

$$EL\phi(x,\omega)=LE\phi(x,\omega)$$

the expectation $E\phi$ solves the elliptic PDE

$$L(E\phi)(x)=(E\rho)(x)$$

This equation has the same form as (1). The equations for the variance and the covariance of a homogenized structure are given in Section 3.

To simplify the analysis, we define the centered charge concentration $\tilde{\rho}$ and the centered potential $\tilde{\phi}$ by

$$\tilde{\rho}:=\rho-E\rho$$
$$\tilde{\phi}:=\phi-E\phi$$

so that $E\tilde{\rho}=0$ and $E\tilde{\phi}=0$ hold. Furthermore, this gives

$$L\tilde{\phi}=\tilde{\rho}$$

and the variance and covariance of the potential and the centered potential are the same, i.e.,

$$\mathrm{cov}\phi=\mathrm{cov}\tilde{\phi}$$
$$\sigma^2\phi=\sigma^2\tilde{\phi}$$

hold.

2.2. Calculation of the Charge Concentration in the Boundary Layer

The calculation of the charge concentration in the boundary layer starts from the atomic structure of the DNA oligomers.[11] To build the single- and double-stranded oligomers, we translate and rotate the known coordinates of the sugar-phosphate backbone and of adenine, cytosine, guanine, or thymine nucleotide. This allows us to construct double helices of arbitrary length and nucleotide sequence. Then the partial charges of the single atoms are obtained from a GROMACS force field.[12]

In the next step, we rotate the axes of the DNA oligomers with respect to the surface and consider these different charge concentrations. A rotation angle of zero degrees corresponds to a double helix that is normal to the surface. The probabilities of the different orientations of the ssDNA (single-stranded DNA) and dsDNA (double-stranded DNA) oligomers are calculated from their electrostatic free energy using a PDE solver, PROPHET. Previously, PROPHET has been applied to solving both equilibrium electrostatics and non-equilibrium transport in bio-electrical systems.[7, 9, 13–15] Here, we briefly outline the computational approach of the orientation probabilities as follows.[14] For each given orientation, the oligomer structure and its partial charges are projected to a three-dimensional simulation grid of 0.2 nm resolution. The interior of the biomolecules is modeled to be inaccessible to mobile ions. The continuity of the electrostatic potential is imposed at the biomolecule and solution interface. The solution of the nonlinear Poisson-Boltzmann equation gives the distribution of the electrostatic potential ϕ, the mobile cation density C^+, and the mobile anion density C^-. Figure 2 shows cross-sectional plots of the simulated electrostatic potential for a dsDNA 12-mer at three different rotation angles, respectively. The bottom surface is charged (0.5 q/nm^2 in this example); its electrical double layer at the specific salt concentration of 30 mM has different overlaps with the charged dsDNA at those rotation angles resulting in different electrostatic interaction energies.

The electrostatic free energy of the system is evaluated by

$$G_{\text{total}} = \int_\Omega \left(\frac{1}{2}\phi(x)(\rho_{\text{f}}(x) + qC^-(x) - qC^+(x)) - k_{\text{B}}T(C^-(x) + C^+(x) - 2C_0) \right) \mathrm{d}x \qquad (2)$$

where ρ_f is the partial charge, C_0 the bulk ionic strength, and Ω the entire system volume. The electrostatic free energy G_{oligomer} of the oligomer and the free energy G_{surface} are calculated separately by using the same approach for isolated oligomer and surface, respectively. Consequently, the free energy of electrostatic interaction is

$$E_{\text{i}} = G_{\text{total}} - G_{\text{oligomer}} - G_{\text{surface}}$$

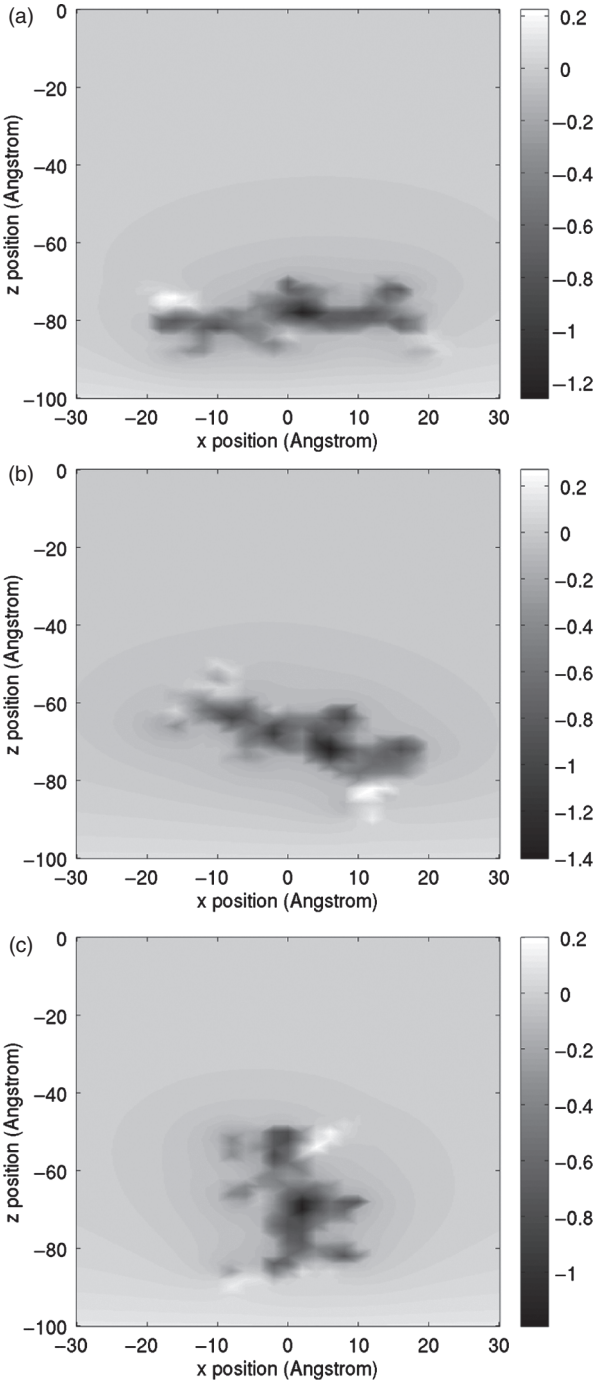

Fig. 2. Cross-sectional plot of the electrostatic potential in V from PROPHET simulations for different rotation angles: (a) 0 degree, (b) 40 degree, and (c) 90 degree. The studied biomolecule is a dsDNA 12-mer, the bottom surface charge density is 0.5 q/nm^2, and the salt concentration is 30 mM.

Then the probability

$$p_{\text{i}} := \frac{\exp(-E_{\text{i}}/(k_{\text{B}}T))}{\sum_{\text{i}} \exp(-E_{\text{i}}/(k_{\text{B}}T))}$$

is assigned to orientation i with the free energy E_{i} according to a Boltzmann distribution.

RESEARCH ARTICLE

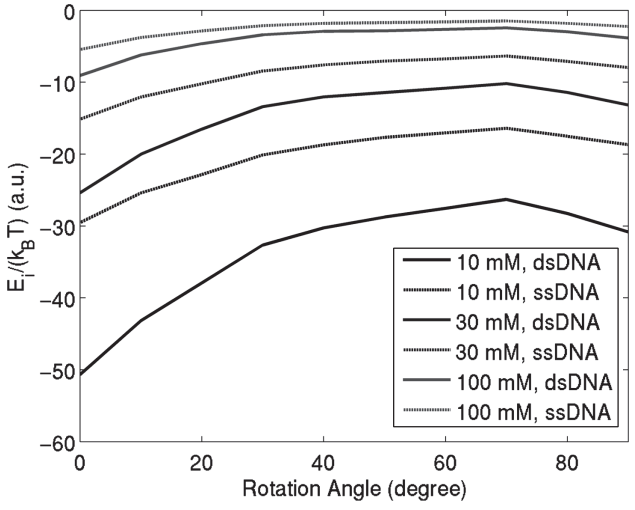

Fig. 3. Simulated interaction electrostatic free energies E_i as functions of biomolecule (ssDNA or dsDNA 12-mers) rotation angles for different salt concentrations. The surface charge density is 0.5 q/nm^2.

An example of simulated E_i as a function of the rotation angle is shown in Figure 3. In the example, ssDNA an dsDNA 12-mers are simulated for different salt concentrations, respectively. The bottom surface charge density is 0.5 q/nm^2. It is found that smaller rotation angles in general result in more negative E_i, indicating that the negatively charged DNA oligomers prefer a parallel orientation with respect to the positively charged bottom surface. However, a small reverse effect is also observed at large angles, which is believed to be due to the effect of the ionic pressure, i.e., the second term in the free-energy equation (2). It is also shown that lower salt concentration or higher biological charge density leads to stronger electrostatic interactions, as expected.

2.3. Calculation of the Current

Having calculated the charge concentrations and their probabilities as above, the expectation $E\phi$ and the variance $\sigma^2\phi$ (and hence also the standard deviation $\sigma\phi$) of the electrostatic potential are calculated in a cross section of the sensor structure. Depending on the orientation of the molecules with respect to the surface, the thickness of the molecule layer is calculated from the double-helix structure of B-DNA and the known total charge is distributed uniformly in the molecule layer. The variance always vanishes at the back gate and at the electrode due to the Dirichlet boundary conditions used on these parts of the boundary. Neumann boundary conditions are used at the rest of the boundaries.

Because $\sigma\phi \ll 1$ holds in the transducer, we can approximate the expected current and its standard deviation by calculating the currents $I(E\phi)$ and $I(E\phi \pm \sigma\phi)$. Since the potential values $\phi(x, y)$ in the (x, y) cross section are known, the graded-channel approximation yields the current through the transducer as

$$I(\phi) = n_i q \mu_p F \int \exp\left(\frac{q\phi_F - q\phi(x,y)}{k_B T}\right) \mathrm{d}x\mathrm{d}y - n_i q \mu_n F \int \exp\left(\frac{-q\phi_F + q\phi(x,y)}{k_B T}\right) \mathrm{d}x\mathrm{d}y$$

where n_i is the intrinsic carrier density of the semiconductor, μ_p and μ_n are the carrier mobilities, and $F = 50$ mV/1 μm is the electric field in longitudinal direction calculated from the source–drain voltage.

3. HOMOGENIZATION RESULTS

The simulation of field-effect biosensors poses a multiscale problem, since the length scale of the whole sensor is orders of magnitude larger than the length scale of a single biomolecule. In this regard, the question arises how the size of fluctuations and noise, i.e., the variance of the solution of the stochastic Poisson-Boltzmann equation, scales with the molecule size. Are small or large molecules favorable with respect to fluctuations and can a simple relationship for the size of the variance be found?

The answers to these questions are summarized in the following. The main result is a PDE whose solution is the covariance of the electrostatic potential. The PDE for the covariance also yields a scaling law for the variance and covariance. The details and the proofs will be published elsewhere.

Three-dimensional structures with a two-dimensional surface and a two-dimensional boundary layer are considered. The coordinate system is chosen so that x_1 is normal to the surface, the surface is located at $x_1 = 0$, and x_2 and x_3 are parallel to the surface. The size of the surface is $x_2 \in [0, L_2]$ and $x_3 \in [0, L_3]$. The boundary layer above the sensor surface is partitioned into cells and each cell k with multi-index $k = (k_2, k_3) \in \{1, \ldots, K_2\} \times \{1, \ldots, K_3\}$ is associated with a random variable ω_k. The charge concentration of cell k is denoted by $\rho_k(x, \omega_k)$ and the random variable ω is defined by $\omega := (\omega_{(1,1)}, \ldots, \omega_{(K_2,K_3)})$.

We make a multi-scale ansatz by writing the charge concentration as

$$\tilde{\rho}_k(x, \omega_k) = \hat{\tilde{\rho}}_k\left(\frac{x_1}{\epsilon}, \frac{x_2 - k_2\epsilon}{\epsilon}, \frac{x_3 - k_3\epsilon}{\epsilon}, \omega_k\right)$$

where $\epsilon \ll 1$ is the scaling factor between slow and fast variables, i.e., it is the ratio between the cell size and the whole domain. We denote the cumulative charge of cell k by

$$R(k, \omega_k) := \int_0^\infty \int_0^{L_2} \int_0^{L_3} \tilde{\rho}_k(y_1, y_2, y_3, \omega_k)\, \mathrm{d}y_3 \mathrm{d}y_2 \mathrm{d}y_1$$

and we also define

$$\bar{R}(\epsilon k_2, \epsilon k_3)^2 := \int_{\Omega_k} R(k, \omega_k)^2 \mathrm{d}P(\omega_k)$$

The following result is deduced after homogenization.

THEOREM 3.1. *The limiting problem for the covariance* $cov\phi = cov\tilde{\phi}$ *of the electrostatic potential as* $\epsilon \to 0$ *is given by*

$$L_\xi L_x(cov\phi)(x,\xi) = \epsilon^4 \delta(x_1, \xi_1, \xi_2 - x_2, \xi_3 - x_3) \times \bar{R}(x_2, x_3)^2$$

where L_ξ *and* L_x *are the differential operator* L *with respect to the* ξ *and* x *variables, respectively. Hence the limiting problem for the variance* $\sigma^2\phi = \sigma^2\tilde{\phi}$ *is given by*

$$L_x^2(\sigma^2\phi)(x) = \epsilon^4 \delta(x_1)\bar{R}(x_2, x_3)^2$$

The proof also yields this corollary.

COROLLARY 3.2. *(Scaling law for the covariance and variance) The covariance* $cov\phi = cov\tilde{\phi}$ *and the variance* $\sigma^2\phi = \sigma^2\tilde{\phi}$ *of the electrostatic potential scale like* ϵ^4 *as* $\epsilon \to 0$.

These results answer the questions posed above. Since ϵ is the ratio between the molecule size (or more precisely, the size of the cells containing the molecules) to the size of the simulation domain, the corollary implies that the variance of the electrostatic potential is much smaller for small molecules than for large molecules all else being equal. Fluctuations and noise, e.g., due to Brownian motion, are therefore much smaller for small molecules and hence these can be detected much more efficiently than larger ones.

4. SIMULATION RESULTS

Simulation results for the nanowire DNA sensor whose structure is shown in Figure 1 are presented. We first define a reference structure and then calculate the fluctuations in the current. Two types of boundary layers are investigated: in the first, each cell is occupied by a single-stranded oligomer and this corresponds to ssDNA detected by (uncharged) PNA receptors or a surface functionalized with ssDNA; in the second type, each cell is occupied by a double-stranded oligomer and this means that an ssDNA target strand is bound to an ssDNA receptor strand.

For the numerical investigations, the reference structure consists of 30 nm of oxide substrate, the nanowire has a cross section of 10 nm · 10 nm, its doping concentration is 10^{18} q/cm^3, its Fermi level is 0.3 V, the oxide thickness is 2 nm, the surface charge density is 0.5 q/ nm^2, the molecules are located at 0.5 nm from the oxide surface, i.e., this distance is the linker length, and the Na^+Cl^- concentration is 30 mM. The cell size is 10 nm · 10 nm, the oligomers consist of 12 nucleotides, and the binding efficiency of the oligomers is 100%. This binding efficiency is consistent with this cell size.[16] The expectation and the standard deviation of the electrostatic potential in the reference structure functionalized with ssDNA are shown in Figure 4.

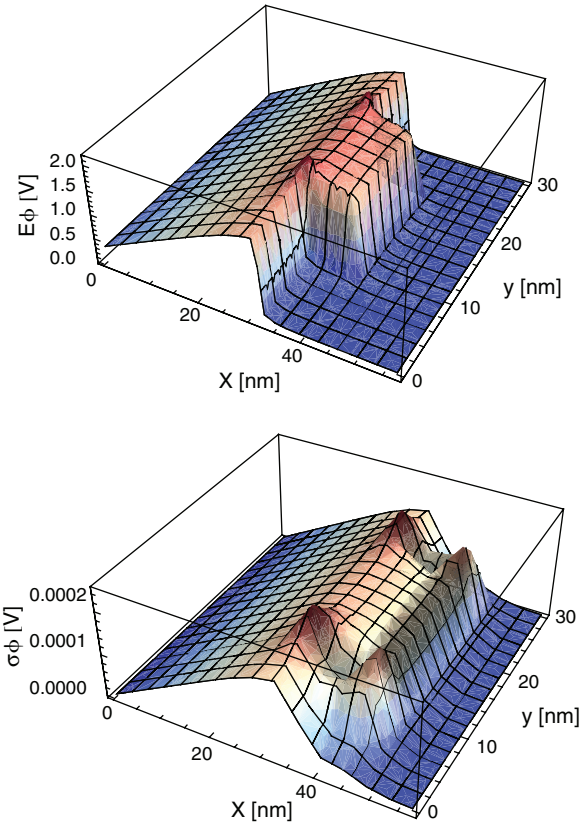

Fig. 4. Expectation $E\phi$ (top) and standard deviation $\sigma\phi$ (bottom) of the electrostatic potential in a cross section of the reference structure functionalized by ssDNA 12-mers. The x-axis is normal to the substrate and the y-axis is parallel to the substrate.

In the following, the fluctuations in the current are shown as the two values

$$\frac{I(E\phi \pm \sigma\phi) - I(E\phi)}{I(E\phi)}$$

i.e., the standard deviation of the current relative to the mean current is calculated.

4.1. Varying Surface Charge

The surface charge is an important parameter of a field-effect sensor. It can be adjusted by chemical means and it determines the operating point of the sensor. In Figure 5, numerical results giving the standard deviation of the current through the sensor relative to the mean current are shown for surface charge densities of 0.2 q/nm^2, 0.5 q/nm^2, and 1.0 q/nm^2. The results imply that the operating point strongly influences the noise level.

In general, it is found that higher surface charge densities lead to stronger DNA-surface binding and therefore less orientation fluctuation, as observed in the Figure 5. It is worth noting the difference between the ssDNA and dsDNA cases. The dsDNA charge is double that of the ssDNA biomolecule, which corresponds to higher current

RESEARCH ARTICLE

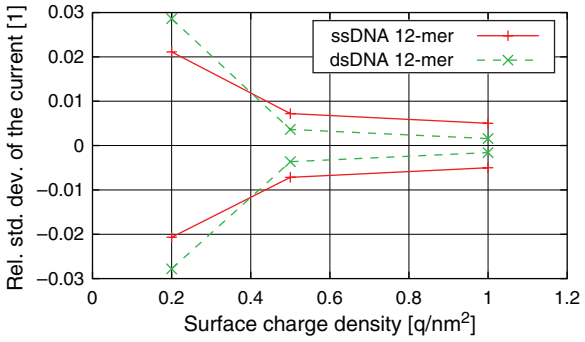

Fig. 5. The standard deviation of the current through the sensor relative to the mean current as a function of surface charge density. Results for 12-mers of ssDNA and dsDNA are shown.

fluctuation at low surface charge density. On the other hand, the stronger binding of dsDNA leads to less orientation fluctuation compared to the ssDNA case. Such a binding energy difference becomes dominant as the surface charge density increases, which explains the observed crossing behavior.

4.2. Varying Ionic Strength

Next, the ionic strength of the electrolyte is varied, while the surface charge density is fixed at 0.5 q/nm^2. Although a lower Na^+Cl^- concentration means less screening of the partial charges of the biomolecules, a certain concentration is necessary for DNA hybridization. In Figure 6, numerical results for the standard deviation are shown for Na^+Cl^- concentrations of 10 mM, 30 mM, and 100 mM. The results show how the ionic strength influences the variance.

As observed in Figure 6, it is found that the variance is generally smallest for low ionic strength, where the electrostatic binding is the strongest. Again, there is a notable difference between the ssDNA and dsDNA cases. For the simulated range of ionic strength, the variance of the dsDNA case is generally smaller compared to that

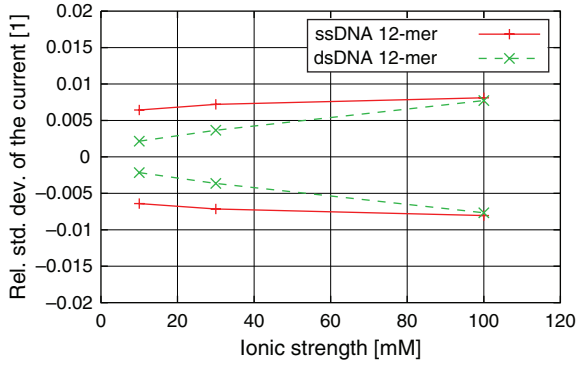

Fig. 6. The standard deviation of the current through the sensor relative to the mean current as a function of the ionic strength of the electrolyte. Results for 12-mers of ssDNA and dsDNA and a surface charge density of 0.5 q/nm^2 are shown.

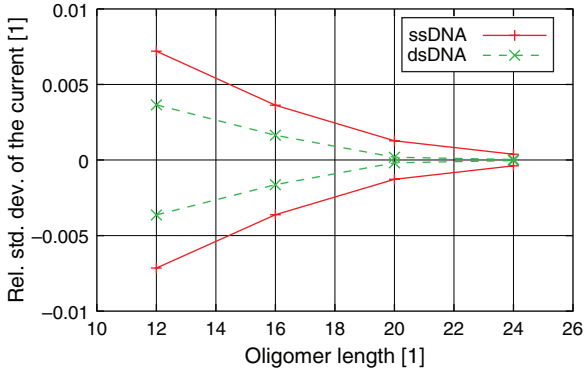

Fig. 7. The standard deviation of the current through the sensor relative to the mean current as a function of oligomer length. Results for ssDNA and dsDNA and a surface charge density of 0.5 q/nm^2 are shown.

of the ssDNA case. Nevertheless, it increases faster as the ionic strength increases and the electrostatic interaction decreases. This is consistent with the interpretation of Figure 5.

4.3. Varying Oligomer Length

Finally, the length of the DNA oligomers is varied for a fixed surface charge density of 0.5 q/nm^2. In the reference structure 12-mers are used, and in Figure 7, results for 12-mers, 16-mers, 20-mers, and 24-mers of ssDNA and dsDNA are shown.

The electrostatic binding increases with the oligomer length, where the parallel orientation of the oligomers becomes more favorable energetically. Therefore the variance is smallest for long oligomers, as observed in Figure 7. These results imply that the oligomer length has a strong influence on the noise level.

Compared to the interpretation of the homogenization result, only the cell size is scaled in Corollary 3.2 all else being equal. In particular, the probabilities of the orientations remain the same as $\epsilon \to 0$. In the numerical simulations, additional information about the molecules is used, since the probability of each DNA oligomer is calculated; these probabilities differ between smaller and larger molecules, while the cell size is the same.

5. CONCLUSION

The simulation capability to calculate fluctuations and noise in nanowire field-effect biosensors was developed based on a PDE model. The model is based on the Poisson-Boltzmann equation for a biomolecule at a charged surface and on the stochastic linearized Poisson-Boltzmann equation for the sensor structure. The model can also be applied to fluctuations and noise due to randomness in charge concentrations in similar structures. In summary, this model makes it possible to calculate the expectation and variance of the electrostatic potential and of the current in the

sensor as functions of the probability distribution of the charge concentrations in the boundary layer where molecular recognition happens in affinity-based sensors.

A scaling law for the variance and covariance of the electrostatic potential was derived by homogenization. The scaling law covers the situation where the size of the molecules in the biofunctionalized boundary layer goes to zero. It implies that the variance of the potential is much smaller for small molecules than for large ones resulting in much reduced fluctuations.

Numerical simulations for a reference DNA-sensor structure were presented and discussed. The effects of varying surface charge, oligomer length, and ionic strength of the electrolyte were investigated. These considerations help in the rational design of field-effect biosensors in order to reduce the fluctuations necessarily present due to Brownian motion.

Acknowledgment: This work was partially (Clemens Heitzinger and Norbert J. Mauser) supported by the ÖAW (Austrian Academy of Sciences) jubilee-fund project *Multi-Scale Modeling and Simulation of Field-Effect Nano-Biosensors* and the FWF (Austrian Science Fund) project P20871-N13 *Mathematical Models and Characterization of BioFETs*.

References

1. J. Hahm and C. M. Lieber, *Nano Lett.* 4, 51 **(2004)**.
2. Y. L. Bunimovich, Y. S. Shin, W.-S. Yeo, M. Amori, G. Kwong, and J. R. Heath, *J. Amer. Chem. Soc.* 128, 16323 **(2006)**.
3. E. Stern, J. F. Klemic, D. A. Routenberg, P. N. Wyrembak, D. B. Turner-Evans, A. D. Hamilton, D. A. LaVan, T. M. Fahmy, and M. A. Reed, *Nature* 445, 519 **(2007)**.
4. G. Zheng, F. Patolsky, Y. Cui, W. U. Wang, and C. M. Lieber, *Nature Biotechnology* 23, 1294 **(2005)**.
5. C. Heitzinger, R. Kennell, G. Klimeck, N. Mauser, M. McLennan, and C. Ringhofer, *J. Phys. Conf. Ser.* 107, 012004/1 **(2008)**.
6. C. Ringhofer and C. Heitzinger, *ECS Transactions* 14, 11 **(2008)**.
7. Y. Liu, K. Lilja, C. Heitzinger, and R. W. Dutton, A simulation study on the effect of electro-diffusion flow, *IEDM 2008 Technical Digest*, San Francisco, CA, USA, December **(2008)**, pp. 491–494.
8. C. Heitzinger, N. Mauser, and C. Ringhofer, *SIAM J. Appl. Math.* **(2009)**, submitted.
9. Y. Liu and R. W. Dutton, *J. Appl. Phys.* 106, 014701 **(2009)**.
10. C. Heitzinger, N. J. Mauser, C. Ringhofer, Y. Liu, and R. W. Dutton, Modeling and simulation of orientation-dependent fluctuations in nanowire field-effect biosensors using the stochastic linearized Poisson–Boltzmann equation, *Proc. Simulation of Semiconductor Processes and Devices (SISPAD 2009),* San Diego, CA, USA, September **(2009)**, p. 86.
11. S. Premilat and G. Albiser, *Nucleic Acids Res.* 11, 1897 **(1983)**.
12. D. van der Spoel, E. Lindahl, B. Hess, A. R. van Buuren, E. Apol, P. J. Meulenhoff, D. P. Tieleman, A. L. T. M. Sijbers, K. A. Feenstra, R. van Drunen, and H. J. C. Berendsen, Gromacs User Manual version 3.3, http://www.gromacs.org **(2006)**.
13. T. A. van der Straaten, J. M. Tang, U. Ravaioli, R. S. Eisenberg, and N. R. Aluru, *J. Comp. Electron.* 2, 29 **(2003)**.
14. A. H. Talasaz, M. Nemat-Gorgani, Y. Liu, P. Ståhl, R. W. Dutton, M. Ronaghi, and R. W. Davis, *Proc. Nat. Acad. Sci. USA* 103, 14773 **(2006)**.
15. Y. Liu, J. Sauer, and R. W. Dutton, *J. Appl. Phys.* 103, 084701 **(2008)**.
16. A. W. Peterson, R. J. Heaton, and R. M. Georgiadis, *Nucleic Acids Res.* 29, 5163 **(2001)**.

Received: 21 July 2009. Accepted: 13 November 2009.